



Impacts of Boundary-Layer Structure and Turbulence on the Variations of PM_{2.5} During Fog–Haze Episodes

Tingting Ju^{1,2} · Bingui Wu² · Hongsheng Zhang³ · Zhaoyu Wang² · Jingle Liu²

Received: 24 May 2021 / Accepted: 20 January 2022 / Published online: 18 February 2022
© The Author(s) 2022

Abstract

The precise cause of PM_{2.5} (fine particulate matter with a diameter smaller than 2.5 μm) explosive growth and the contribution of intermittent turbulence to the dispersion of PM_{2.5} are uncertain. Thus, the impact of boundary-layer structure and turbulence on the variations of surface PM_{2.5} during fog–haze episodes, especially during explosive growth and dispersion episodes, are investigated using turbulence data collected at a 255-m high meteorological tower in Tianjin from 2016 to 2018. Results suggest that the explosive growth of surface PM_{2.5} during fog–haze episodes is closely related to weak turbulent mixing, nocturnal inversions, or anomalous inversions, and the barrier effect of strong turbulent intermittency. Turbulent intermittency acts as a lid for hindering pollutant dispersion and is favourable for the fast accumulation of surface PM_{2.5}. Apart from the potential causes mentioned above, the persistent moderate south-westerly flow is also a contributing factor for the explosive growth of surface PM_{2.5} during fog–haze episodes associated with regional transport. In addition, we demonstrate a possible mechanism of how intermittent turbulence affects the dispersion of PM_{2.5}. Results verify that intermittent turbulence induced by the nocturnal low-level jet (LLJ) indeed plays an important role in the dispersion of PM_{2.5}. However, the contribution of intermittent turbulence generated by the nocturnal LLJ to the dispersion of PM_{2.5} strongly relies on the intensity of the nocturnal LLJ.

Keywords Barrier effect · Boundary-layer structure · Haze · Intermittent turbulence · PM_{2.5} explosive growth

✉ Bingui Wu
tjwbgtjwbgt@126.com

¹ Navigation College, Dalian Maritime University, Dalian 116026, China

² Tianjin Key Laboratory for Oceanic Meteorology, Tianjin Institute of Meteorological Science, Tianjin Meteorological Bureau, Tianjin 300074, China

³ Laboratory for Climate and Ocean-Atmosphere Studies, Department of Atmospheric and Oceanic Sciences, School of Physics, Peking University, Beijing 100871, China

1 Introduction

Visibility is the farthest distance at which the human eye can distinguish a target against a background (Duntley 1948). During recent years, haze and fog have frequently caused severely low visibility in the North China Plain (NCP; Quan et al. 2011). Haze and fog, which can significantly affect transportation (Fabbian et al. 2007; Chen et al. 2012), human health (Kim et al. 2019), and the economy (Gultepe et al. 2007), and have attracted considerable public attention (Chen et al. 2013).

Aerosol particles, especially the $PM_{2.5}$ (fine particular matter with a diameter smaller than $2.5 \mu\text{m}$), are the main cause of hazy weather (Ji et al. 2012; Zhang et al. 2012). With the rapid urbanization and tremendous economic development during the past decades, hazy weather associated with $PM_{2.5}$ has become the foremost pollution issue in China (Ding and Liu 2014), particularly in the NCP (Hu et al. 2014; Ye et al. 2015b). Fog is a boundary-layer weather phenomenon composed of suspended water droplets or crystals, which can reduce horizontal visibility to much less than 1 km (WMO 1992). Previous literature has reported that the economic and human losses associated with fog events are comparable to those caused by tornadoes and even hurricanes and winter storms (Gultepe et al. 2007), and fog events have caused costly and even catastrophic events in China. Haze and fog frequently and simultaneously occur in the NCP (Ju et al. 2020a); thus, much attention should be paid to fog–haze events (Fu et al. 2014).

Despite the decreased number of foggy–hazy days in the NCP in recent years (Tao et al. 2014), fog–haze events characterized by extremely high mass concentration of $PM_{2.5}$ still frequently occurred there (Zhao et al. 2013; Zhang et al. 2015). To understand the potential causes of fog–haze events in China, the physical, chemical, and optical properties of aerosol particles and meteorological conditions during haze episodes have been widely investigated (Zhao et al. 2013; Han et al. 2018; Liu et al. 2019). These studies reveal that the occurrence of a fog–haze event is strongly affected by source emissions (Wang et al. 2013; Liu et al. 2014), production of secondary pollutants, and meteorological conditions (Tang et al. 2016; Li et al. 2019), which include constant stagnant flow, strong stable stratification, and weak turbulent mixing (Zhang et al. 2015; Miao et al. 2018).

Fog–haze events usually form under strong stable stratification, with stagnant flow and weak turbulence (Ye et al. 2015b). The stable boundary layer (SBL) is typically characterized by intermittent turbulence or even no turbulence at a variety of heights, temporal scales, and spatial locations (Mahrt 1998; Van de Wiel et al. 2003; Salmond 2005). The term intermittency has different meanings that vary among studies (Coulter and Doran 2002; Acevedo et al. 2006; Mahrt 2007). Mahrt (1989) defines intermittency as the case where eddies at all scales are missing or suppressed at scales that are greater than those for large eddies. Several studies have indicated that intermittency is driven by non-stationarity due to motions on time scales that are slightly greater than turbulence (Mahrt 2010) when the large-scale flow is weak. These motions are referred to as submesoscale motions (Sun et al. 2004; Anfossi et al. 2005). Therefore, turbulent mixing during fog–haze episodes cannot be calculated with the eddy-correlation method when intermittent turbulence exists because of the non-stationarity imposed by submesoscale motions (Vickers and Mahrt 2006; Acevedo et al. 2007). Additionally, most investigations (Petäjä et al. 2016) focus on the feedback between aerosols, turbulent mixing, and the boundary layer, with little discussion on the dynamic effect of turbulence on the transport of particulate matter, not to mention the intermittent turbulence under strongly stable conditions (Wei et al. 2018). A series of works (Vindel and Yagüe 2011; Helgason and Pomeroy 2012) have confirmed that intermittent turbulence

accounts for significant vertical momentum, and heat and mass exchange between the surface and the upper boundary layer, implying that intermittent turbulence may be one of the key factors in pollutant dispersion. Therefore, to analyze the nonlinearity and non-stationarity of intermittent turbulence in the SBL, a new technique, the so-called arbitrary-order Hilbert spectral analysis (arbitrary-order HSA) method proposed by Huang et al. (2008), is used. The arbitrary-order HSA method has been successfully applied in analyses of turbulence in the SBL (Wei et al. 2016, 2017). Although early studies have explored some potential reasons for fog–haze, there are few works focusing on the effects of intermittent turbulence in the SBL.

The impacts of boundary-layer structure and turbulence on the variations of $PM_{2.5}$ during fog–haze events are still ambiguous due to the unclear impacts of intermittent turbulence and the lack of continuous and comprehensive field observations. The purpose of the present study is to reveal the impacts of boundary-layer structure and turbulence on the variations of $PM_{2.5}$ during fog–haze episodes, especially on the explosive growth and dispersion of surface $PM_{2.5}$. It should be kept in mind that our aim is not to compare the advantages and disadvantages of different methods, but to obtain pure turbulent quantities and study the intermittent turbulence in the SBL with the aid of an effective method. In Sect. 2, the observation site, instruments, and dataset are described. Moreover, the criteria for haze and fog are also introduced. In Sect. 3, the calculations of turbulent quantities and methods used are presented. Section 4 contains discussions of our results in detail, including an overview of the fog–haze events, the behaviour of intermittent turbulence during fog–haze episodes, and the impacts of boundary-layer structure and intermittent turbulence on the explosive growth and dispersion of $PM_{2.5}$ during fog–haze episodes. In Sect. 5, conclusions are summarized.

2 Data and Criteria

2.1 Experiment Site and Data

Tianjin (39.08°N, 117.21°E; altitude 3.4 m) is the largest coastal city in the NCP, with the Bohai Sea to the east. Due to the rapid urbanization in recent decades, Tianjin has a typical urban underlying terrain (Ye et al. 2015a). In this study, data are mainly obtained from a 255-m high meteorological tower, which is located at the meteorological observation station (ABLTJ, 54,517) to the south of Tianjin city (Fig. 1). There are no tall buildings around the tower within a radius of 50 m, and the heights of the surrounding buildings within 300 m are less than 30 m. The routine surface observations, such as visibility, rainfall, and relative humidity, are obtained from the surface automatic weather station (AWS) at the same site. The $PM_{2.5}$ mass concentration is obtained from a tapered element oscillating microbalance (TEOM, RP1405D, Thermo Fisher Scientific, Waltham, Massachusetts, USA), which weighs dry aerosols rather than aerosols that have absorbed water. The wind-profile data are obtained from the 1363 MHz boundary-layer wind-profile radar (Radian CFL-06, Beijing Institute of Radio Measurement, Beijing, China) at Xiqing in Tianjin (XQTJ). Xiqing station (39°5′20″N, 117°3′56″E), which is nearly 14 km to the west of the 255-m high meteorological tower (Fig. 1), is the only surface AWS included in the global climate observing system in Tianjin operated by the China Meteorological Administration (CMA).

Measurements of meteorological parameters at the 255-m tower and the AWS were recorded automatically and continuously at a 1-min interval. Considering the time interval of turbulence fluxes, the 1-min interval meteorological parameters are processed with

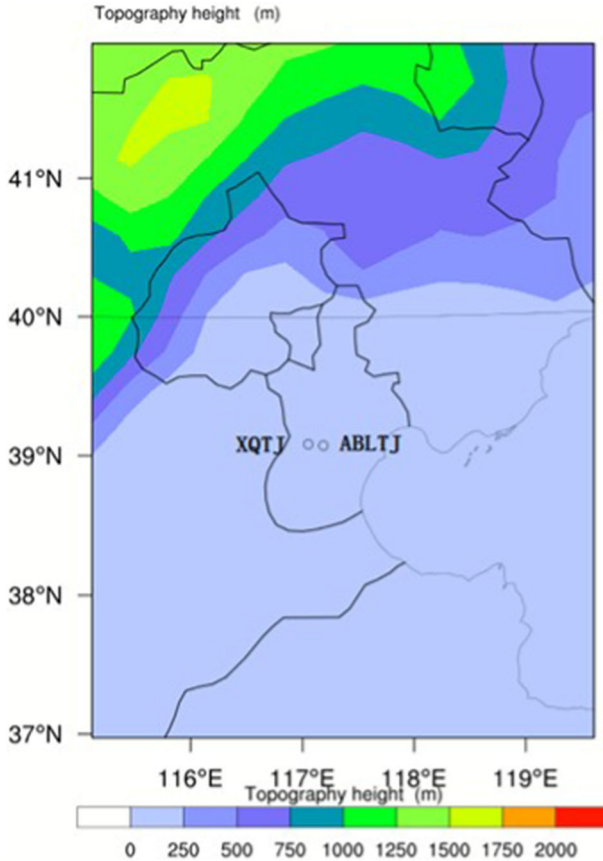


Fig. 1 Topographic image of measurement stations including the Xiqing station (XQTJ) and the meteorological observation station (ABLTJ) in Tianjin

a moving average of 30-min interval. The sampling frequency of atmospheric turbulence data is 10 Hz, and preprocessing is performed using Eddy Pro software (Advanced 4.2.1, LI-COR Biosciences, Inc., Lincoln, Nebraska, U.S.A.). The preprocessing includes spike removal, double coordinate rotation, and trend removal. In addition, the block time-average method is used in the trend removal process, with an averaging time interval of 30 min. Since the eddy-correlation results depend on wind speed, the stability, and friction velocity, strict quality control is performed on the atmospheric turbulence data as follows. Any data that met any of the following criteria (Ye et al. 2015a) were discarded: (1) the angle between the vertical and horizontal wind components greater than $\pm 7^\circ$, (2) the mean wind speed less than 0.2 m s^{-1} , and (3) the friction velocity less than 0.01 m s^{-1} . For detailed information about the site and data background refer to Ju et al. (2020b). To obtain the boundary-layer wind-profile data, the radar wind-profile radar located at Xiqing station, which operates at a frequency of 1363 MHz with three observation models, is used. The detailed descriptions of the wind-profile radar characteristics are shown in Table 1 in Wu et al. (2020).

Table 1 Information about the two fog–haze events

Information or variables	Case 1	Case 2
Starting time (LT) of Haze	1900 on 11 November 2018	1600 on 24 November 2018
End time (LT) of Haze	1300 on 15 November 2018	1600 on 27 November 2018
Starting time of fog (LT)	0300 on 14 November 2018	0100 on 26 November 2018
Duration of fog (h)	5	26
Mean PM _{2.5} concentration ($\mu\text{g m}^{-3}$)	140	210

2.2 Criteria for Fog and Haze

Visibility degradation is always related to a high level of aerosol number concentration and relative humidity (Elias et al. 2009; Deng et al. 2011); therefore, visibility and relative humidity (RH) are usually criteria for identifying fog. However, the critical value of RH is not identical in the published literature (Li et al. 2011; Ding and Liu 2014). In this study, the criteria for fog are as follows (Ye et al. 2015a): (1) $RH \geq 90\%$, (2) precipitation fog is beyond the scope, and 3) the 10-min visibility < 1 km. According to the observations and forecasting levels of haze published by the CMA (QX/T113-2010), when the mass concentration of PM_{2.5} is larger than $75 \mu\text{g m}^{-3}$ and the $RH < 90\%$, this can be identified as a haze event. Based on this, only the haze events with a duration longer than 24 h are considered. Fog frequently forms during the long-term haze events in the NCP; thus, if fog occurs during the haze episode, it is defined as a fog–haze event.

3 Methodology

3.1 Calculation of Turbulent Quantities

Turbulent quantities including turbulence kinetic energy (TKE) and variances of two horizontal velocity components u , v as well as the vertical velocity component w (m s^{-1}) are calculated according to

$$TKE = \frac{1}{2}(\overline{u'^2} + \overline{v'^2} + \overline{w'^2}), \quad (1)$$

$$\sigma_u^2 = \overline{u'^2}, \quad (2)$$

$$\sigma_v^2 = \overline{v'^2}, \quad (3)$$

$$\sigma_w^2 = \overline{w'^2}, \quad (4)$$

where u' , v' , and w' are fluctuating values with respect to average values of u , v and w . Turbulence data, including variables TKE , σ_u , σ_v , and σ_w , are averaged over 30-min intervals.

3.2 Automated Algorithm to Identify the Spectral Gap

Turbulent intermittency is defined as eddies at all scales being missing or suppressed at scales that are greater than those for large eddies (Mahrt 1999). Turbulent intermittency is driven

by non-stationarity due to motion on time scales that are slightly greater than turbulence (Mahrt 2010) when the large-scale flow is weak. To obtain the actual turbulent quantities and quantify the strength of the local turbulent intermittency, an automated algorithm (Ren et al. 2019a), which is based on arbitrary-order HSA method (Huang et al. 2008; Wei et al. 2016), is used. The automated algorithm can identify the spectral gap and has been applied in turbulence analysis in the SBL (Ren et al. 2019a, b). The arbitrary-order HSA method developed based on the Hilbert–Huang transform (Huang et al. 1998) has been widely used to deal with nonlinear and non-stationary time series. The arbitrary-order Hilbert spectrum is as follows,

$$Lq(\omega) = \int p(\omega, A)A^q dA, \tag{5}$$

where $q \geq 0$ is the arbitrary moment, ω stands for the instantaneous frequency, A represents the instantaneous amplitude, and $p(\omega, A)$ is the joint probability density function.

The spectral gaps are inspected by studying the second-order Hilbert spectra (marginal spectrum) of turbulence deviations such as u' , v' , and w' for each 30-min interval. Moreover, based on the arbitrary-order Hilbert spectrum (Eq. 5), the arbitrary-order Hilbert marginal spectrum is calculated as

$$H(\omega) = \int p(\omega, A)A^2 dA. \tag{6}$$

The spectral gap between the submesoscale motion and turbulence is confirmed as the interval of frequency in which values of the second-order Hilbert spectra are approximately constant, or the slope is approximately equal to zero. Figure 2 shows the second-order Hilbert spectra from the newly reconstructed and raw data. As shown in Fig. 2a, the lower-frequency limit of the spectral gap for u is $\omega = 0.008$ Hz, and the upper-frequency limit is not used to reconstruct the data. The part of the frequency larger than ω indicates the turbulence signal, and the part of the frequency smaller than ω indicates nonstationary motion, which has a scale larger than that for turbulence.

The strength of turbulence in the acquired signal can be indicated by using the ratio of the turbulent intensity to that of all signals. The velocity scale of submesoscale motion represents the kinetic energy of submesoscale motion and is stated as follows,

$$V_{\text{smeso}} = \sqrt{u'^2_{\text{smeso}} + v'^2_{\text{smeso}} + w'^2_{\text{smeso}}}, \tag{7}$$

where u'_{smeso} , v'_{smeso} , and w'_{smeso} represent the deviations reconstructed from the intrinsic mode function (corresponding to the submesoscale motion during each 30-min period). Similarly, the turbulent velocity scale is calculated as

$$V_{\text{turb}} = \sqrt{u'^2_{\text{turb}} + v'^2_{\text{turb}} + w'^2_{\text{turb}}}, \tag{8}$$

where u'_{turb} , v'_{turb} , and w'_{turb} stand for the deviations reconstructed from the intrinsic mode function corresponding to the turbulent motion during each 30-min period.

Intermittency can be defined by the turbulent and non-turbulent portions of a signal once the criteria for identifying the boundary between them have been established (Salmond 2005). To identify the strength of turbulent intermittency, an effective index, called the local intermittent strength of turbulence (*LIST*), is used and calculated as

$$LIST = \frac{V_{\text{turb}}}{\sqrt{V_{\text{smeso}}^2 + V_{\text{turb}}^2}}. \tag{9}$$

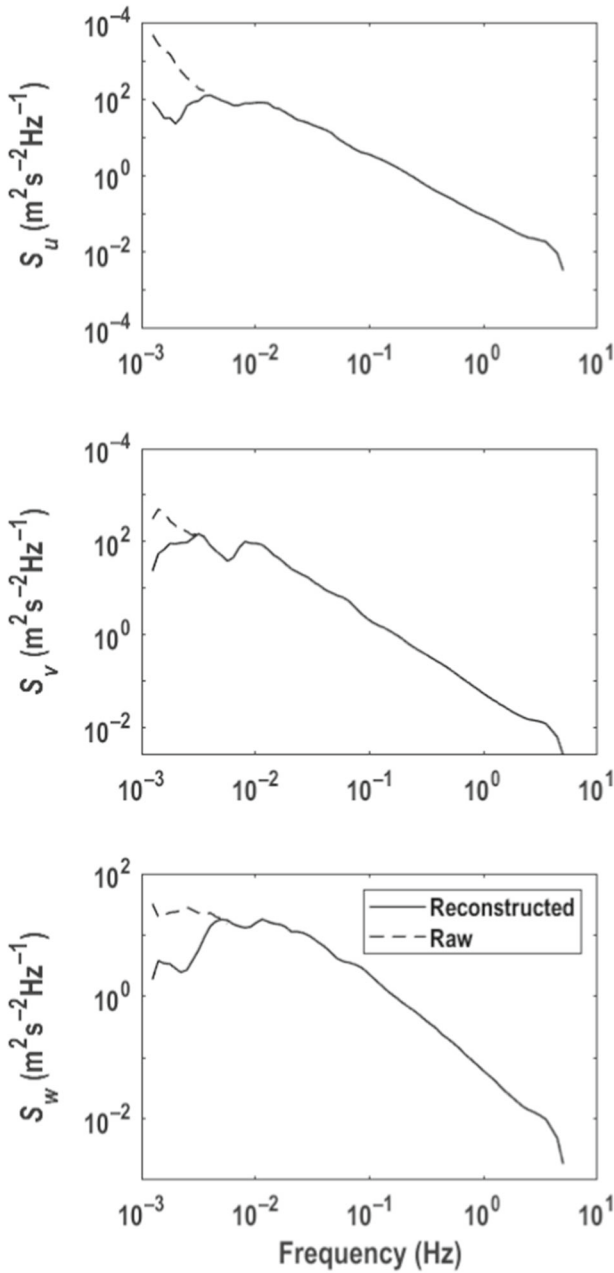


Fig. 2 Second-order Hilbert spectra of the three velocity components **a** u , **b** v at 0500 LT (local time = UTC + 8 h), and **c** w at 0430 LT at 40 m on 14 November 2018 in Tianjin. The black dotted line indicates the spectra from the raw data, and the solid black line indicates the spectra from the reconstructed data for pure turbulence

The parameter $LIST$ can be obtained based on examining the spectral gap and reconstructing the turbulence data reasonably by using the Hilbert–Huang transform. A large deviation from $LIST = 1$ indicates that the effect of submesoscale components cannot be neglected, and the local intermittency is strong. However, as the parameter $LIST$ cannot represent the intensity of the intermittency alone, the intensity of turbulent mixing (TKE or σ_w), u' , v' , and w' also should be taken into account to describe the turbulent intermittency.

4 Results and Discussions

Statistical results show haze frequently occurred in Tianjin (approximately 37%) from 2016 to 2018, while the occurrence frequency of haze in winter was over 50%. Moreover, approximately 79% of fog events in Tianjin occurred during the haze episodes, indicating that fog and haze events frequently and simultaneously appeared in the NCP. Therefore, two fog–haze events occurring in 2018, which are termed as case 1 and case 2 (Table 1) hereinafter, are chosen to investigate the effects of boundary-layer structure and turbulence on the variations of surface $PM_{2.5}$ during fog–haze episodes.

4.1 Overview of the Two Fog–Haze Events

Figure 3 illustrates the time series of different variables during the two fog–haze events, including surface visibility, RH , specific humidity (q), temperature, wind speed, wind direction, $PM_{2.5}$ mass concentration, and TKE . All variables were observed at the surface except for TKE , which was observed at 40 m. Due to the installation height limitation of the sonic instrument, the surface turbulence is represented by turbulence at 40 m. Moreover, it should be kept in mind that values of TKE were all calculated using pure turbulent fluctuations based on the HSA method, as explained in Sect. 4.3. The wind speed and turbulence kinetic energy were always low during fog–haze episodes, with the values being 0.80 m s^{-1} (0.82 m s^{-1}) and $0.38 \text{ m}^2 \text{ s}^{-2}$ ($0.44 \text{ m}^2 \text{ s}^{-2}$) during case 1 (case 2). The daily mean $PM_{2.5}$ mass concentrations during case 1 and case 2 were approximately 140 and $210 \mu\text{g m}^{-3}$, respectively. Fog (shaded area) during case 1 occurred from 0300 to 0700 LT (local time = UTC + 8 h) on 14 November 2018, with the duration being 5 h. Fog (shaded area) during case 2 occurred from 0100 LT on 26 November to 0300 LT on 27 November. There were obvious negative correlations between visibility and RH as well as surface $PM_{2.5}$ mass concentration (Fig. 2a1, a2, c1, c2) during the two cases, which confirms that low visibility in Tianjin is closely related to the occurrence of fog–haze (Ye et al. 2015b; Ju et al. 2020a).

4.2 Weather Scenario Analysis

To analyze the atmospheric background fields of the two fog–haze events, surface and 925-hPa synoptic charts during the two fog–haze episodes are presented in Fig. 4. The weather conditions were similar before the occurrence of the two fog–haze events, with a surface high-pressure system in the western region of the NCP (Fig. 4a, e). The Tianjin region was affected by an anticyclone and was controlled by a stagnant wind field, resulting in unfavourable transport conditions. The low wind speeds at the surface and high elevations suggest that the occurrence of the haze was mainly due to local emissions.

For case 1, haze occurred at 1900 LT on 11 November due to the local emissions and stagnant wind fields. Subsequently, the Tianjin region was affected by high pressure at 2000

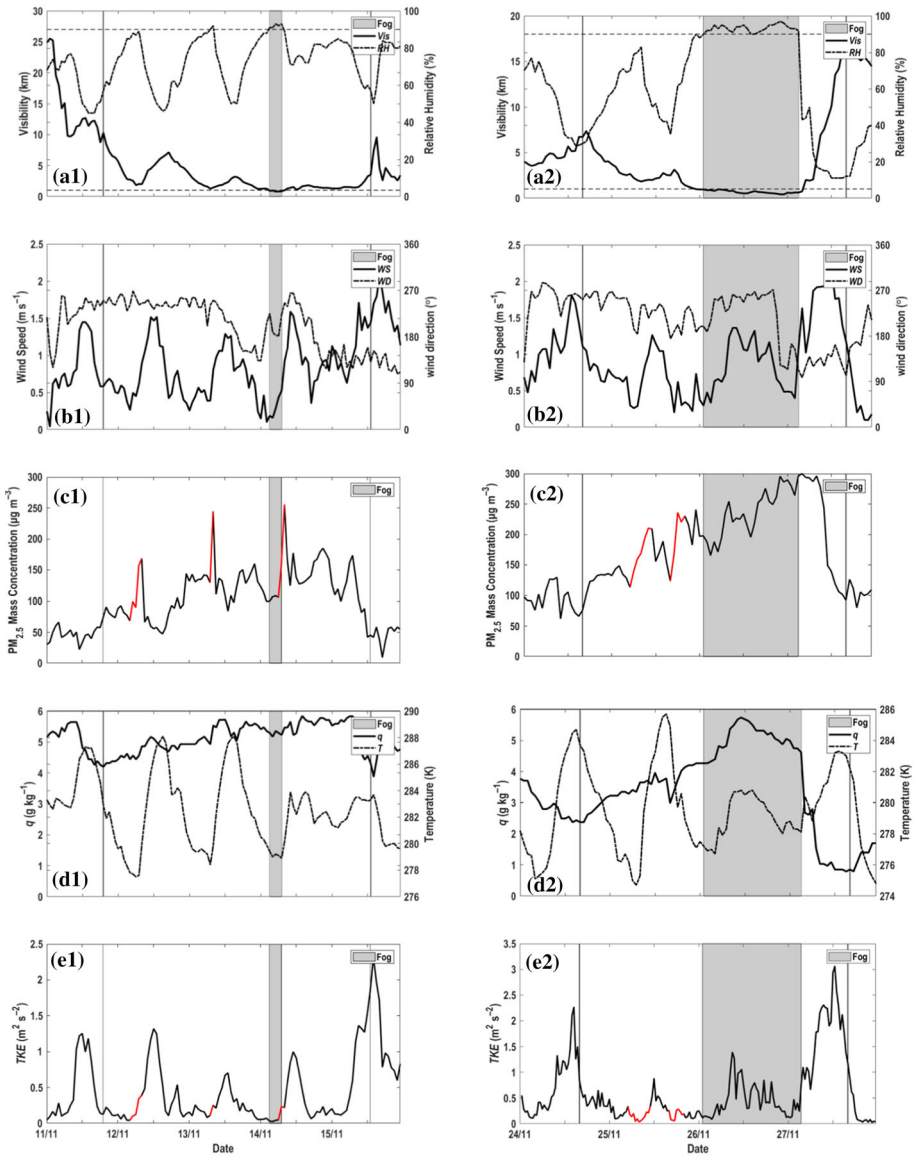


Fig. 3 Temporal variations of **a1** visibility, *RH*, **b1** wind speed, wind direction, **c1** $PM_{2.5}$ mass concentrations, **d1** specific humidity, temperature, and **e1** *TKE* during case 1 (from 0000 LT on 11 November to 2350 LT on 15 November). All variables were observed at the surface except for *TKE*, which was observed at 40 m. Shaded areas denote the fog episodes. Solid black lines from left to right denote the starting and end time of the fog–haze, respectively. Black dotted lines from top to bottom in panel **a1** and **a2** indicate that the *RH* is equal to 90% and the visibility is equal to 1 km. Red lines represent the surface $PM_{2.5}$ explosive growth episodes. The right column **a2–f2** is the same as the left column **a1–f1**, but for case 2

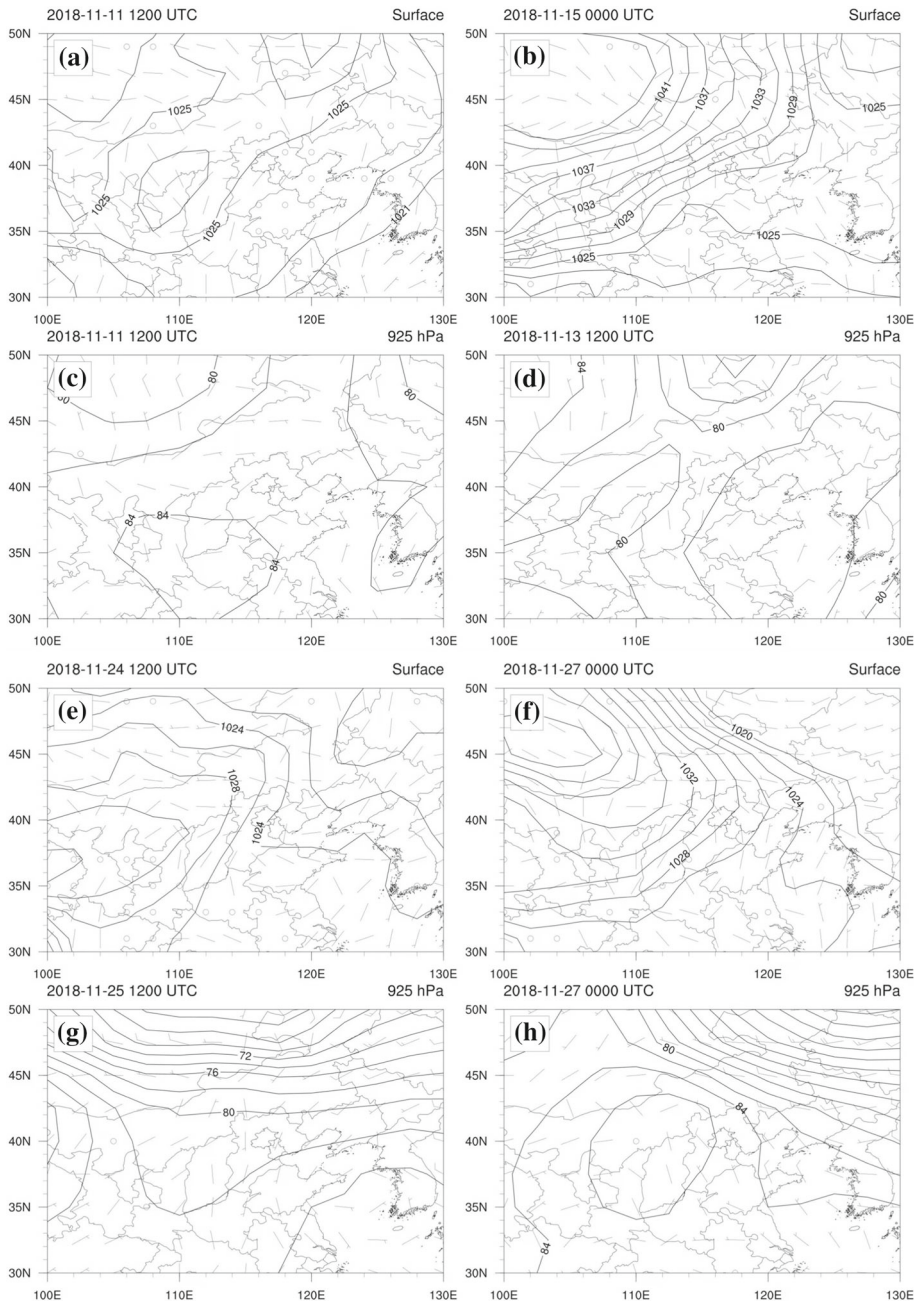


Fig. 4 Surface weather conditions at **a** 1200 UTC on 11 November and **b** 0000 UTC on 15 November, and 925-hPa weather conditions at **c** 1200 UTC on 11 November and **d** 1200 UTC on 13 November. Surface weather conditions at **e** 1200 UTC on 24 November and **f** 0000 UTC on 27 November, and 925-hPa weather conditions at **g** 1200 UTC on 25 November and **h** 0000 UTC on 27 November. The atmospheric circulation background data are obtained from National Center for Environmental Prediction Final Operational Global Analysis (1 by 1 grids, <https://rda.ucar.edu/datasets/ds083.2/>)

LT on 13 November (Fig. 4d), and fog formed in the early morning of 14 November. On the morning of 14 November, the thin fog dissipated due to solar radiation; however, haze characterized by high mass concentration of $PM_{2.5}$ persisted. On the morning of 15 November, the Tianjin region was affected by an anticyclone in the north-western region of the NCP, as shown in Fig. 4b. The fog–haze dissipated due to the strong north-westerly wind, which carried clear and dry air to Tianjin.

For case 2, the occurrence of the haze event was also mainly due to the local emissions, while the maintenance of the fog–haze was somewhat different from that of case 1. Haze occurred at 1600 LT on 24 November due to the local emissions and stagnant wind fields. From 2000 LT on 25 November, the Tianjin region was affected by a surface low-pressure system, and synoptic weather conditions at 925 hPa show that the Tianjin region lay ahead of the trough (Fig. 4g). Consequently, a persistent south-westerly flow brought polluted air masses and water vapour to Tianjin, which led to the continuous increase in $PM_{2.5}$ mass concentration (Fig. 3c2) and specific humidity (Fig. 3d2). The fog persisted for the whole day with the aid of moist advection (Tian et al. 2019; Ju et al. 2020a). Finally, the Tianjin region was affected by an anticyclone in the north-western region (Fig. 4f), and the fog–haze dissipated because of the strong north-westerly wind. In a nutshell, haze during case 2 also formed mainly due to the local emissions and stagnant wind fields. While from 2000 LT on 25 November, the maintenance of fog–haze can be partly attributed to regional transport. In summary, the trends of the weather systems during the formation and dissipation stages of the two fog–haze events are relatively similar.

4.3 Characteristics of Boundary-Layer Structure and Turbulence During Fog–Haze Episodes

Figure 5 depicts the profiles of the daily mean potential temperature (θ) and the mean change of θ ($\Delta\theta$) during the two fog–haze episodes at 15 different heights. The mean change of θ at a given height was calculated by subtracting the mean value of θ during the two fog–haze episodes from that on the clear days (24 h before the occurrence of the fog–haze). Results of the daily mean potential temperature show that though the height of the inversion layer changed slightly, the intensity of the inversion layer gradually increased during fog–haze episodes (Fig. 5a1, a2). A profile of $\Delta\theta$ during a case 1 (Fig. 5b1) shows that the mean potential temperature at the upper layer (160–250 m) during a fog–haze episode was higher than that on a clear day ($\Delta\theta > 0$). Though the mean potential temperature at the lower layer (from surface to 160 m) during fog–haze episode was lower than that on a clear day ($\Delta\theta < 0$), the intensity of the inversion layer still increased during fog–haze episode. The profile of $\Delta\theta$ during a case 2 (Fig. 5b2) shows that the mean potential temperature during a fog–haze episode was always higher than that on a clear day ($\Delta\theta > 0$), and the warming of the upper layer (160–250 m) was greater than that of the lower layer (from surface to 160 m), which also verifies that the intensity of the inversion layer increased during the fog–haze episode. Compared with case 1, the mean potential temperature in the lower layer (from surface to 160 m) was higher than that on a clear day, and the intensity of the inversion layer was stronger during case 2. In a nutshell, results of the boundary-layer structure confirm that the two fog–haze events both occurred in the SBL, and the intensities of the inversion layer during fog–haze episodes were stronger than those on clear days.

Due to the important roles of turbulence in the transport of heat, moisture, and pollutants, the impacts of turbulence on the variations of surface $PM_{2.5}$ during fog–haze episodes have attracted considerable public attention. However, the impacts of turbulence on the variations

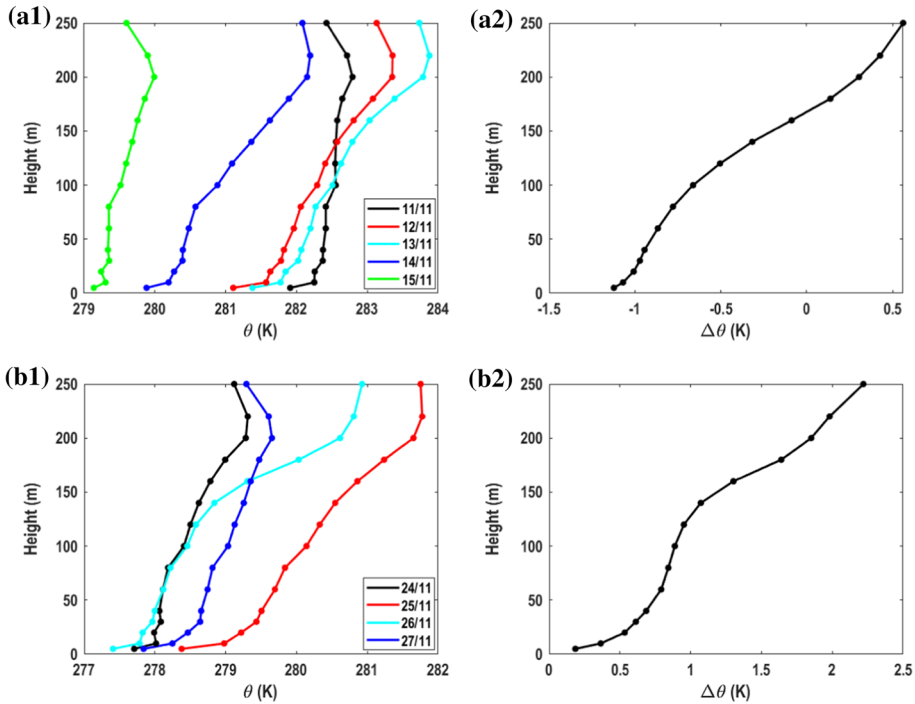


Fig. 5 Profiles of the daily mean potential temperature (θ) during **a1** case 1 and **a2** case 2. Profiles of change of θ during the **b1** case 1 and **b2** case 2

of surface $\text{PM}_{2.5}$ during fog–haze episodes are still not yet clearly understood. Results of the boundary-layer structure confirm that fog–haze events both formed in the SBL, in which turbulent mixing is weak and typically characterized by intermittent turbulence (Salmond 2005; Wei et al. 2018; Ren et al. 2019a). During fog–haze episodes, exchanges between the surface and the atmosphere calculated with the eddy-correlation method may be questionable due to the non-stationarity imposed by submesoscale motions (Acevedo et al. 2006, 2007; Ren et al. 2019a). Therefore, the original results, which are calculated via the classic eddy-correlation system, and the new results, calculated using the HSA method, of the variable TKE and the variance parameters (σ_u , σ_v , and σ_w) during fog–haze episodes are compared (Fig. 6). Obvious overestimations of the variable TKE calculated by the eddy-correlation method (original results) are observed, with the slope of the fitted line being 0.86 and 0.89 for case 1 (Fig. 6a) and case 2 (figures omitted here). The traditional eddy-correlation method also overestimates by approximately 10% (6%) and 10% (10%) for the quantities of σ_u and σ_v during case 1 (case 2). There are almost no discrepancies between the original results and the new results of σ_w (Fig. 6d), which confirms that the appearance of the spectral gap has fewer effects on the variance in the vertical velocity component. Results show that overestimations of turbulent quantities calculated by the eddy-correlation method due to intermittent turbulence cannot be neglected during fog–haze episodes; thus, values of the variable TKE presented here were all calculated using pure turbulent fluctuations based on the HSA method. In addition, the impacts of intermittent turbulence on the variations of surface $\text{PM}_{2.5}$ during fog–haze episodes are the focus here.

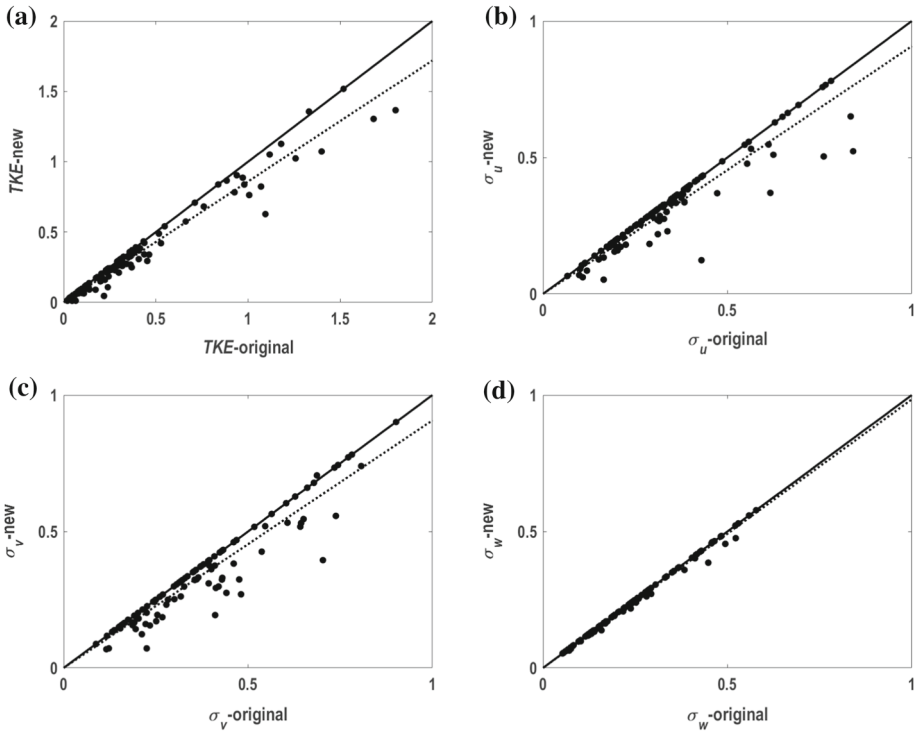


Fig. 6 Comparisons of **a** TKE , **b** σ_u , **c** σ_v , and **d** σ_w from new 30-min results with those from original results during the case 1. The solid black line represents the 1:1 line, while the black dotted line represents the fitted results during the fog–haze episode

4.4 Impacts of Boundary-Layer Structure and Turbulence on the Variations of Surface $PM_{2.5}$

The analysis of atmospheric background fields suggests that the occurrence and maintenance of fog–haze during case 1 were mainly due to the local emissions and stagnant wind fields. There is no large pollution source around our experimental station, and there was no significant emission variability during the studied episodes; thus, the variations of surface $PM_{2.5}$ concentration during case 1 were deemed to be closely related to the meteorological conditions, including constant stagnant winds, strong stable stratification, and weak turbulent mixing (Zhang et al. 2015; Miao et al. 2018; Li et al. 2019). In our study, we mainly focused on the relationships between the boundary-layer structure as well as turbulence and the explosive growth of surface $PM_{2.5}$, which is defined as $PM_{2.5}$ mass concentration that at least doubled in several hours to 10 h (Zhong et al. 2018). The explosive growths of surface $PM_{2.5}$ were observed in the early morning of 12, 13, and 14 November (red lines in Fig. 3c1); however, the precise cause of $PM_{2.5}$ explosive growth is still uncertain. Persistent weak southerly winds facilitated local pollutants accumulation by minimizing horizontal pollutant diffusion. Local emissions under weak winds were likely conducive but not dominant with respect to the explosive growths of surface $PM_{2.5}$.

The potential causes of the explosive growth of surface $PM_{2.5}$ concentration have been analyzed previously. Wang et al. (2018) report that the aerosol–radiation feedback and the

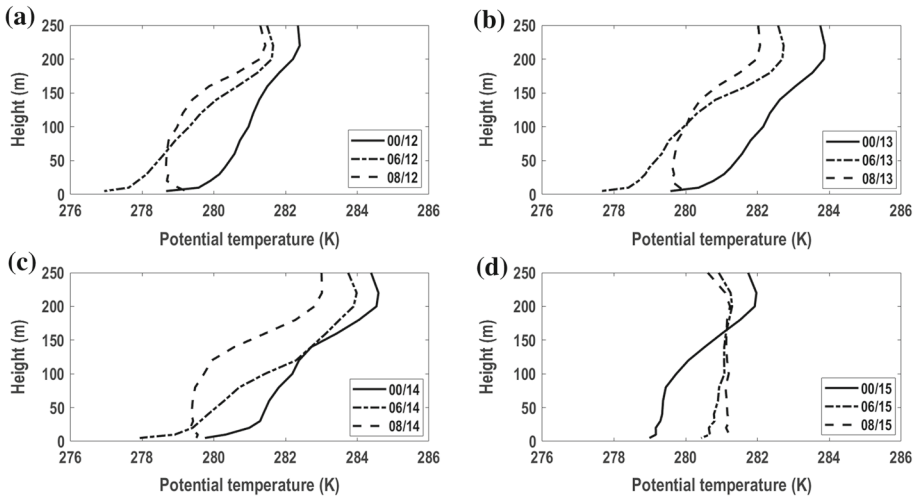


Fig. 7 Profiles of potential temperature at 0000, 0600, and 0800 LT on **a** 12, **b** 13, **c** 14, and **d** 15 November

decrease in the turbulent diffusion are favourable for the explosive growth of $PM_{2.5}$. The boundary-layer structure (Fig. 7) suggests that the explosive growths of surface $PM_{2.5}$ during case 1 all occurred in the SBL; however, the correlations between *TKE* and surface $PM_{2.5}$ concentration are extremely poor during the explosive growth episodes of surface $PM_{2.5}$ (Fig. 3c1, e1). The explosive growth of surface $PM_{2.5}$ during case 1 was even accompanied by slightly increasing weak turbulent mixing (red lines in Fig. 3e1), indicating the decrease in the turbulent diffusion was not the main cause of the $PM_{2.5}$ explosive growth during case 1. Zhong et al. (2018) point out that the explosive growth of surface $PM_{2.5}$ concentration is dominated by a near-ground anomalous inversion and moisture accumulation in the daytime. However, the explosive growth of surface $PM_{2.5}$ was frequently observed in the early morning. Though pollutants consistently accumulated accompanied by the near-ground inversion throughout the night-time, the explosive growth of surface $PM_{2.5}$ was not observed at night. Thus, aerosol–radiation feedback and near-ground inversion were also not the main causes of the surface $PM_{2.5}$ explosive growth during case 1.

Apart from the potential causes mentioned above, the increase in humidity also facilitated aerosol hygroscopic growth and secondary formation by heterogeneous reactions, which were also favourable for increasing surface $PM_{2.5}$ concentration. However, the $PM_{2.5}$ mass concentrations are obtained from a TEOM device, which weighs dry aerosols rather than aerosols that have absorbed water. Though the formation of secondary aerosols was likely conducive to the increase in surface $PM_{2.5}$, it was not dominant with respect to the explosive growth of surface $PM_{2.5}$ concentration (Sun et al. 2014). Therefore, besides the causes documented previously, there must be other physical mechanisms leading to the explosive growth of surface $PM_{2.5}$. As mentioned above, fog–haze events frequently occurred in the SBL, in which turbulent mixing was weak and typically characterized by intermittent turbulence. Therefore, the impacts of intermittent turbulence on the explosive growth of surface $PM_{2.5}$ are studied.

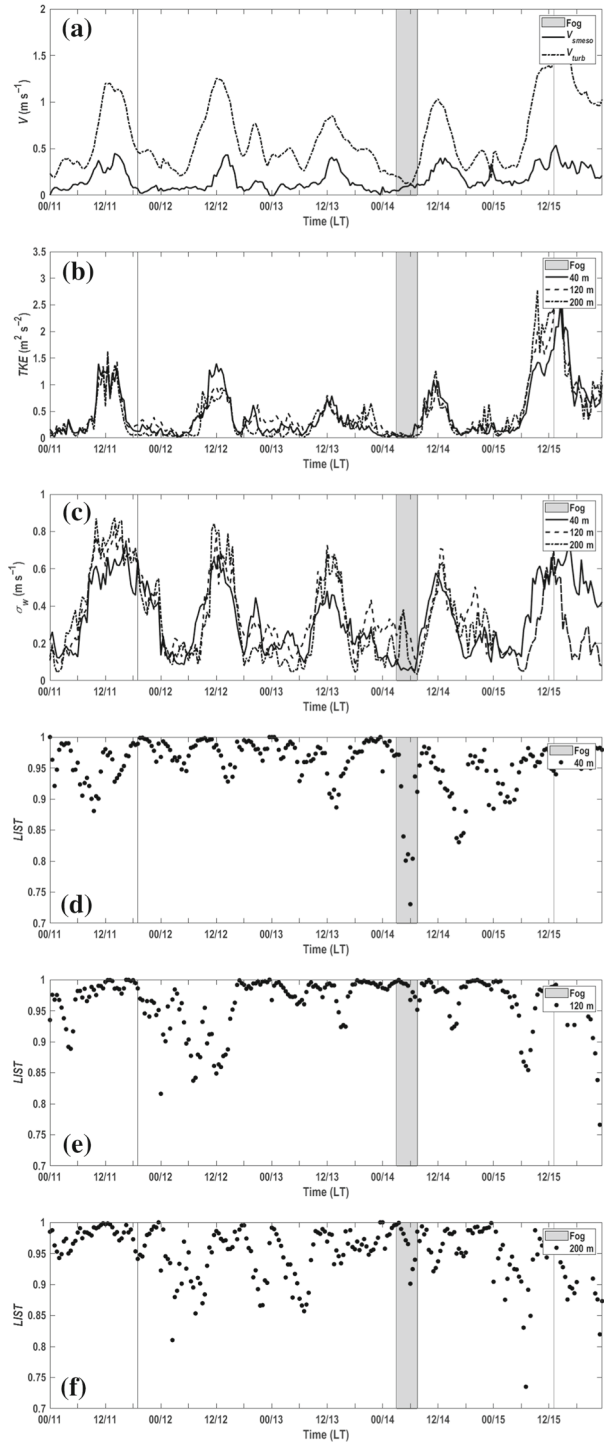
Businger (1973) proposed a cyclic process of intermittent turbulence in the near-surface layer under ideal conditions: when the thermal stability of the near-surface layer increases rapidly, the turbulence in the near-surface layer is suppressed, collapses, and appears as

laminar flow at a certain height. The atmosphere and the underlying surface decouple because turbulent transport weakens or even disappears. Then, due to high-level weather-scale wind shear, intermittent increasing turbulence appears and transmits downward. The intermittent turbulence weakens the stratification effect, and the coupling between the atmosphere and the underlying surface is re-established (Businger 1973). According to Businger's theory, turbulence at certain heights may disappear, forming a laminar flow as if there is a barrier layer that hinders the transmission of turbulence. This phenomenon is beneficial for understanding the physical mechanism responsible for the rapid accumulation of pollutants and is defined as the turbulence 'barrier effect' by Ren et al. (2021). In our study, the parameter *LIST*, which refers to the proportion of turbulent components in the collected 30-min signal, is adopted to identify the strength of turbulent intermittency.

The temporal variations of V_{smeso} , V_{turb} at 40 m, *TKE*, σ_w , and *LIST* at 40, 120, and 200 m during case 1 are presented in Fig. 8. During the surface $\text{PM}_{2.5}$ explosive growth episode on 12 November, the turbulent mixing at the entire tower layer was weak (Fig. 8b, c). Strong turbulent intermittency (low value of *LIST*) was observed in the early morning of 12 November at 120 and 200 m (Fig. 8e, f). As mentioned above, the weak turbulent mixing and low value of *LIST* manifest the suppression of turbulent motion by sub-mesoscale motion in the early morning of 12 November. The turbulence in the near-surface layer was suppressed, collapsed, and a laminar flow appeared at 120 or 200 m, which is the so-called barrier effect. Therefore, we deem that there was an inversion lid at 120 or 200 m, and the substance exchange was suppressed under this condition. Ultimately, the weak turbulent mixing in stable stratification and the barrier effect of strong turbulent intermittency facilitated the rapid accumulation of surface $\text{PM}_{2.5}$ and led to the explosive growth of surface $\text{PM}_{2.5}$. Analogous phenomena were also observed in the early morning of 13 and 14 November. In the early morning of 14 November, the value of V_{smeso} at 40 m gradually increased (Fig. 8a), while the value of V_{turb} was inhibited (Fig. 8a), resulting in the low values of *LIST* (Fig. 8d). Weak turbulent mixing and the barrier effect of strong turbulent intermittency also resulted in the explosive growth of surface $\text{PM}_{2.5}$ in the early morning of 14 November. In a nutshell, the explosive growth of surface $\text{PM}_{2.5}$ observed in the early morning of 12, 13, and 14 November can be partly attributed to the weak turbulent mixing and the barrier effect of strong turbulent intermittency in the near-surface. However, the turbulent mixing in the SBL was always weak, and the explosive growth of surface $\text{PM}_{2.5}$ was not always observed. The analysis suggests that to state the impacts of turbulence on the variations of $\text{PM}_{2.5}$ during fog-haze episodes, intensities of turbulent mixing (*TKE* or σ_w) and turbulent intermittency (*LIST*) both should be taken into account.

Moreover, it is worth noting that there was intermittent turbulence at 200 m in the early morning of 13 November (Fig. 9a, b, c). Some potential causes of intermittent turbulence in the SBL that have been documented include gravity waves (Sorbján and Czerwinska, 2013), solitary waves (Terradellas et al. 2005), horizontal meandering of the mean wind field (Anfossi et al. 2005), and low-level jets (LLJs, Marht 2014; Wei et al. 2018). Based on criteria for LLJs in Tianjin documented in previous studies (Wei et al. 2014; Wu et al. 2020), simplified criteria, the maximum wind speed ($V_{\text{max}} \geq 6 \text{ m s}^{-1}$), and the difference between V_{max} and the minimum wind speed above or the wind speed at the height of 3 km $\geq 3 \text{ m s}^{-1}$, were used. Intermittent turbulence in the early morning of 13 November was induced by wind shear associated with a nocturnal LLJ (Fig. 9d). The result confirms that the nocturnal LLJ is a potential source of turbulence in the SBL. However, the intensity of intermittent turbulence was weak, and the time scale of turbulent bursts was very short, resulting in the turbulent mixing being still weak. Wei et al. (2018) have pointed out that the intermittent turbulent fluxes associated with the nocturnal LLJ contribute positively to the

Fig. 8 Temporal variations of **a** V_{smeso} , V_{turb} at 40 m, **b** TKE , **c** σ_w at 40 m, 120 m, and 220 m, and $LIST$ at **d** 40 m, **e** 120 m, and **f** 220 m from 0000 LT on 11 November to 2350 LT on 15 November. Solid black lines from left to right denote the starting and end time of the fog–haze, respectively. Shaded area denotes the fog episode



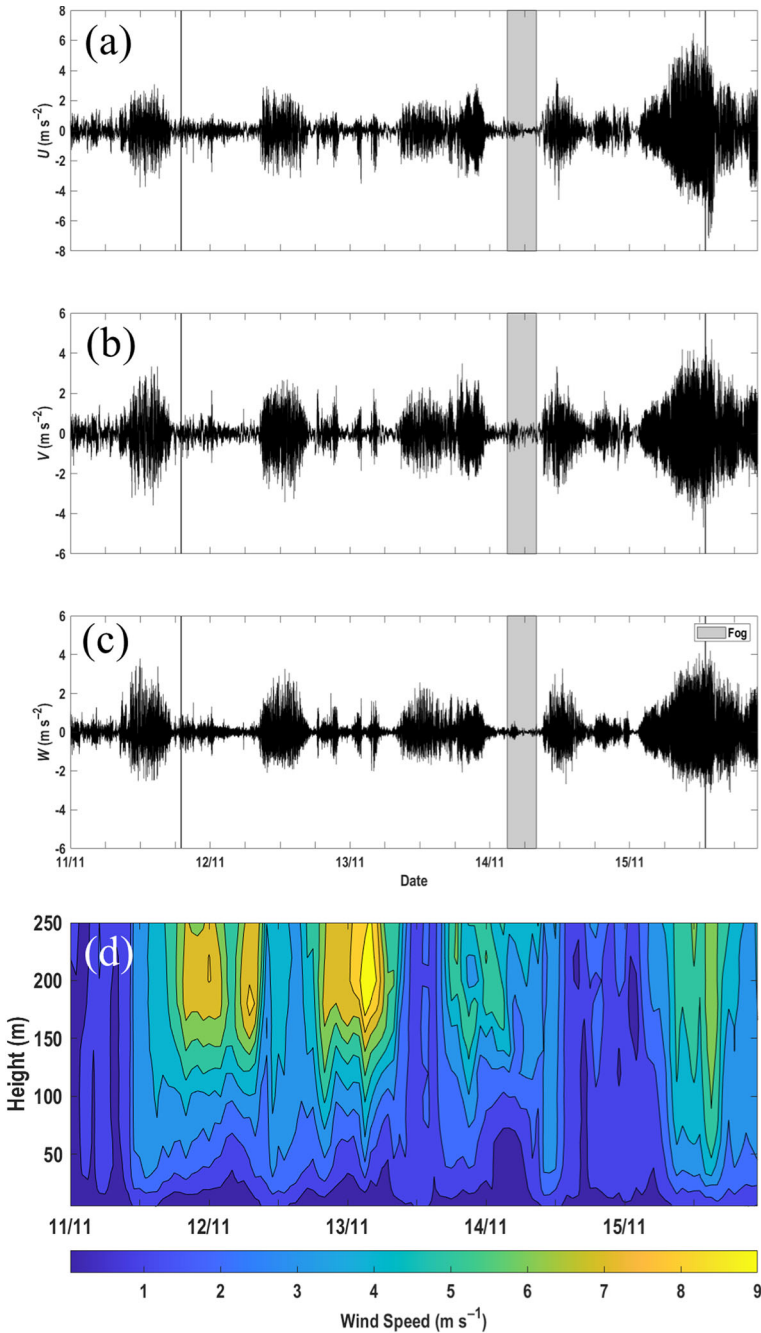


Fig. 9 Temporal variations of **a** u , **b** v , and **c** w at 200 m from 0000 LT on 11 November to 2350 LT on 15 November. Solid black lines from left to right denote the starting and end time of the fog–haze, respectively. Shaded area denotes the fog episode. **d** Profiles of wind speed from 0000 LT on 11 November to 2350 LT on 15 November

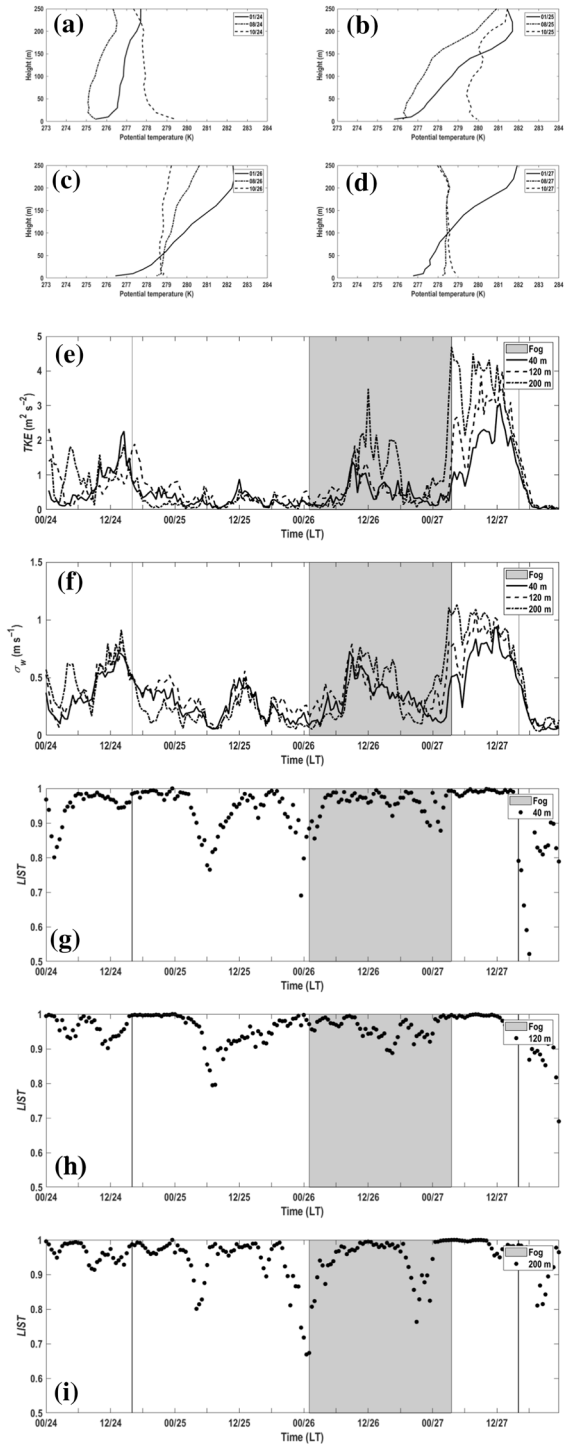
vertical transport of particulate matter and improve the air quality near the surface. However, the intermittent turbulence induced by the weak nocturnal LLJ in the early morning of 13 November was weak (Fig. 8b, c), resulting in the $PM_{2.5}$ changing slightly. Since the intensity of intermittent turbulence induced by the LLJ is closely related to the intensity of the LLJ (Banta et al. 2006), the impact of intermittent turbulence induced by the nocturnal LLJ on the dispersion of particulate matter strongly relies on the intensity of the nocturnal LLJ.

A significant decrease in surface $PM_{2.5}$ concentration was observed from 0800 LT on 12, 13, and 14 November. Due to surface heating, the strong stable stratification collapsed (Fig. 7), and the barrier effect of strong turbulent intermittency at the near-surface disappeared. The increasing turbulence induced by surface heating weakens the stratification, and the coupling between the atmosphere and the underlying surface is re-established (Businger 1973). Therefore, the significant decrease in surface $PM_{2.5}$ concentration after the explosive growth episode was mainly due to the increasing turbulent mixing (Fig. 8b, c) with weak intermittency (Fig. 8d, e, f). As shown in Fig. 4b, on the morning of 15 November, the Tianjin region lay ahead of the cold high-pressure system, which was located in the north-west of Tianjin. The strong north-westerly wind, which carried clear and dry air to Tianjin, led to the dissipation of the haze. At the same time, strong turbulent mixing with weak intermittency associated with solar radiation and wind shear were also favourable for the dispersion of $PM_{2.5}$.

As mentioned in Sect. 4.2, before 2000 LT on 25 November, the occurrence and maintenance of haze during case 2 were also mainly due to local emissions and stagnant wind fields. The variations of surface $PM_{2.5}$ concentration before 2000 LT on 25 November were also closely related to the meteorological conditions, including constant stagnant winds, strong stable stratification, and weak turbulent mixing. Surface $PM_{2.5}$ explosive growth was observed on the morning of 25 November (red lines in Fig. 3c2). Persistent weak southerly winds facilitated local pollutant accumulation; however, weak southerly winds on the morning of 25 November was likely conducive but not dominant with respect to the explosive growths of surface $PM_{2.5}$. Moreover, the turbulent mixing at the entire tower layer was weak (Fig. 10e, f) and there were no pronounced correlations between the turbulent mixing and the explosive growth of surface $PM_{2.5}$ (Fig. 3c2, e2). The boundary-layer structure shows that there was a near-ground anomalous inversion on the morning of 25 November (Fig. 10b). There are two factors, including advection and radiation, that cause the occurrence of the inversion above Tianjin. Advection inversion was closely related to the wind speed; however, the analysis of atmospheric background fields and wind-profile data suggest that the anomalous inversion appearing on the morning of 25 November was accompanied by weak winds. Thus, the advection was not striking, and the contribution of advection to the anomalous inversion was limited. The radiation cooling at the surface was favourable for a nocturnal inversion but not dominant with respect to the anomalous inversion in the morning. Aerosol scattering (Wang et al. 2014; Gao et al. 2015) resulted in a significant reduction in shortwave irradiance at the ground, which further reduced near-ground temperature. These findings indicate that the anomalous inversion on the morning of 25 November can be partly attributed to the radiation cooling effect of pre-existing aerosols. Although a high concentration of $PM_{2.5}$ was frequently observed in the autumn and winter of Tianjin, an anomalous inversion was not always observed, indicating the potential causes of anomalous inversions still need to be revealed by further studies. The anomalous inversion trapped polluted air beneath it and facilitated pollutant accumulation by suppressing vertical air mixing and reducing the boundary-layer height (Fig. 10; Zhong et al. 2018).

Moreover, strong turbulent intermittency (low value of *LIST*) was observed on the morning of 25 November at 40, 120, and 200 m (Fig. 10g, h, i). Therefore, a laminar flow appeared at 40,

Fig. 10 Profile of potential temperature at 0100, 0800, and 1000 LT on **a** 24, **b** 25, **c** 26, and **d** 27 November. Temporal variations of **e** TKE , and **f** σ_w at 40 m, 120 m, and 220 m, and $LIST$ at **g** 40 m, **h** 120 m, and **i** 220 m from 0000 LT on 24 November to 2350 LT on 27 November



120, or 200 m, indicating that there was a lid at 40, 120, or 200 m, and the pollutants exchange is suppressed. Ultimately, the weak turbulent mixing, the barrier effect of strong turbulent intermittency, and the anomalous inversion facilitated the rapid accumulation of surface $\text{PM}_{2.5}$ and led to the explosive growth of surface $\text{PM}_{2.5}$ on the morning of 25 November.

Synoptic weather conditions at 925 hPa show that from 2000 LT on 25 November, the Tianjin region lay ahead of the trough (Fig. 4h), and after this time, the explosive growth of surface $\text{PM}_{2.5}$ concentration was observed (Fig. 3c2). Persistent south-westerly winds brought polluted air masses and water vapour to Tianjin, which led to the continuous increase in $\text{PM}_{2.5}$ mass concentration (Fig. 3c2) and specific humidity (Fig. 3d2). Boundary-layer structure and turbulence data show that there was a near-ground inversion, and the turbulent mixing at the entire tower layer was weak, which was favourable for the accumulation of $\text{PM}_{2.5}$. Moreover, strong turbulent intermittency (low value of $LIST$) was observed on the night of 25 November at 40 and 200 m (Fig. 10g, i). The barrier effect of strong turbulent intermittency also facilitated the accumulation of $\text{PM}_{2.5}$. Therefore, the persistent moderate south-westerly winds, the weak turbulent mixing under the stable stratification, and the barrier effect of strong turbulent intermittency led to the explosive growth of surface $\text{PM}_{2.5}$ on the night of 25 November.

In summary, the potential causes of the surface $\text{PM}_{2.5}$ explosive growth during fog–haze episodes in the present study are various, including weak turbulent mixing, nocturnal inversion/anomalous inversion, regional transport, and the barrier effect of strong turbulent intermittency. The analogous result that weak turbulent mixing with strong turbulent intermittency leads to the explosive growth of surface $\text{PM}_{2.5}$, was also observed from another two fog–haze events in 2016 (figures omitted here).

At 2100 LT on 26 November, $LIST$ at 200 m gradually increased from low values to 1, and a turbulent burst formed at 200 m (Fig. 11c). The turbulent burst was also induced by wind shear associated with the nocturnal LLJ (figure omitted here), and the intermittent increasing turbulence transmitted downward to the surface, resulting in the increase of turbulent mixing at lower levels (Fig. 11a, b, c). The intermittent increasing turbulence weakens the stratification stability (Fig. 10d), and the coupling between the atmosphere and the underlying surface is re-established. Compared with the weak LLJ ($V_{\max} < 9 \text{ m s}^{-1}$) in the early morning of 13 November during case 1, the intensity of LLJ on the night of 26 November and in the early morning of 27 November during the case 2 was much stronger (approximately 15 m s^{-1}), resulting in the turbulent bursts and turbulent mixing being stronger during case 2. The strong intermittent turbulent mixing contributed positively to the dispersion of pollutants and improved visibility near the surface. Results suggested that intermittent turbulence induced by the nocturnal LLJ indeed plays an important role in the variations of $\text{PM}_{2.5}$; however, the impact of intermittent turbulence induced by the nocturnal LLJ on the dispersion of $\text{PM}_{2.5}$ strongly relies on the intensity of the nocturnal LLJ.

5 Conclusions

The analysis of the boundary-layer structure confirms that fog–haze events always form in the SBL, in which turbulence is typically characterized by intermittency. Thus, the impact of boundary-layer structure and turbulence on the variations of surface $\text{PM}_{2.5}$ during fog–haze episodes are investigated. In particular, the impacts of intermittent turbulence on the explosive growth and dispersion of surface $\text{PM}_{2.5}$ are focused on using the turbulence data collected at a 255-m tower in Tianjin from 2016 to 2018.

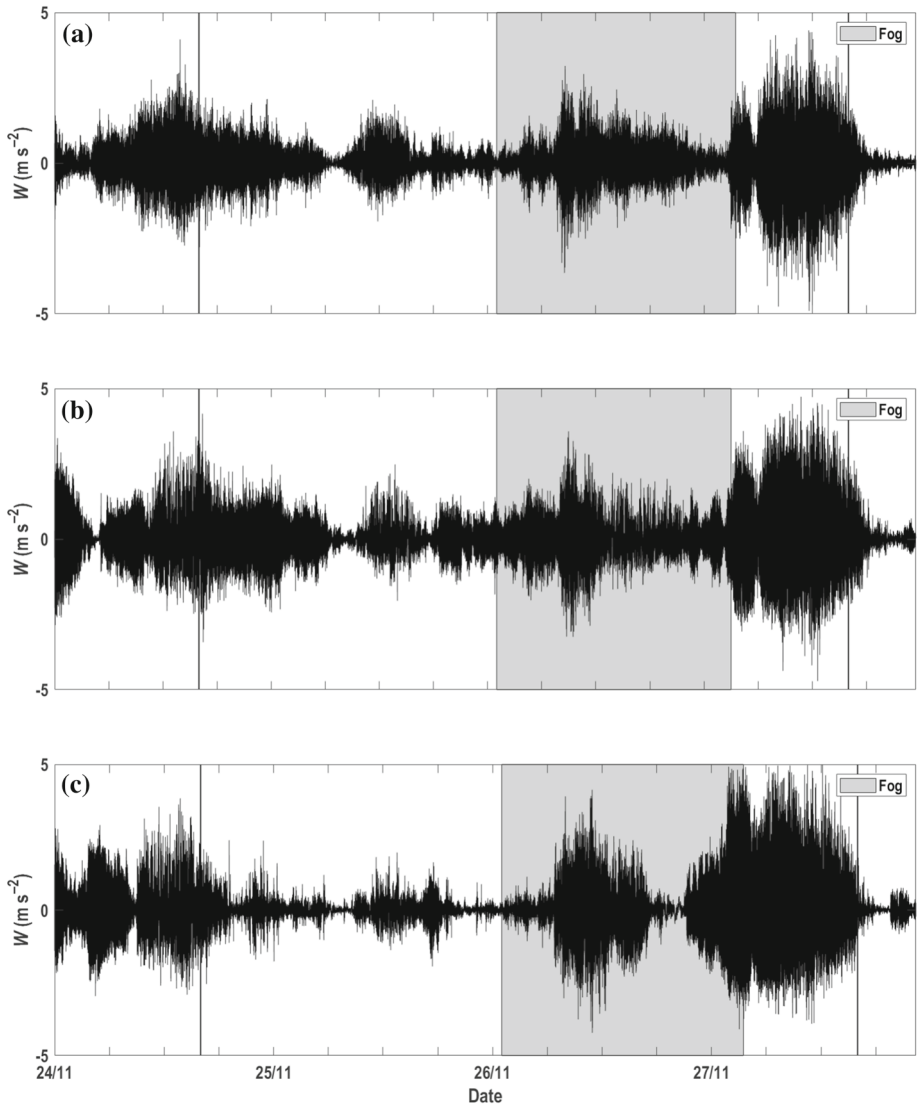


Fig. 11 Temporal variations of w' at **a** 40 m, **b** 120 m, and **c** 200 m from 0000 LT on 24 November to 2350 LT on 27 November. Solid black lines from left to right denote the starting and end time of the fog–haze, respectively. Shaded area denotes the fog episode

The analysis of atmospheric background fields suggests that the occurrence and maintenance of haze during case 1 are mainly due to the local emissions and stagnant wind fields. Therefore, the variations of surface $PM_{2.5}$ concentration are closely related to the meteorological conditions, including boundary-layer structure and turbulence. Results show that the potential causes of the surface $PM_{2.5}$ explosive growth during fog–haze episodes are various, including weak turbulent mixing, a nocturnal inversion or anomalous inversion, and the

barrier effect of strong turbulent intermittency. Strong turbulent intermittency, which indicates that turbulence at certain heights is inhibited or disappears, forming a laminar flow as if there is a barrier layer, hinders pollutants dispersion and facilitates the fast accumulation of surface $PM_{2.5}$. Apart from the potential causes mentioned above, the persistent moderate south-westerly flow is also a contributing factor for the explosive growth of surface $PM_{2.5}$ during fog–haze episodes associated with regional transport. The results suggest that, to state the impacts of turbulence on the variations of $PM_{2.5}$ during fog–haze episodes, intensities of turbulent mixing (TKE or σ_w) and turbulent intermittency ($LIST$) both should be taken into account.

In addition, results verify that intermittent turbulence induced by the nocturnal LLJ indeed plays an important role in the variations of $PM_{2.5}$. The intermittent increasing turbulence induced by the nocturnal LLJ can transport downward and weaken the stratification stability, contributing positively to the vertical transport of $PM_{2.5}$ and improving the air quality near the surface. However, the impact of intermittent turbulence induced by the nocturnal LLJ on the dispersion of $PM_{2.5}$ strongly relies on the intensity of the nocturnal LLJ. This work has demonstrated a possible mechanism of how intermittent turbulence affects the dispersion of pollutants.

Acknowledgements This work was jointly funded by the National Natural Science Foundation of China [42105084, 41675018, 41805028]; and the Scientific Research Fund for Talents of Dalian Maritime University [02500117].

Open Access This article is licensed under a Creative Commons Attribution 4.0 International License, which permits use, sharing, adaptation, distribution and reproduction in any medium or format, as long as you give appropriate credit to the original author(s) and the source, provide a link to the Creative Commons licence, and indicate if changes were made. The images or other third party material in this article are included in the article's Creative Commons licence, unless indicated otherwise in a credit line to the material. If material is not included in the article's Creative Commons licence and your intended use is not permitted by statutory regulation or exceeds the permitted use, you will need to obtain permission directly from the copyright holder. To view a copy of this licence, visit <http://creativecommons.org/licenses/by/4.0/>.

References

- Acevedo OC, Moraes OLL, Degrazia GA, Medeiros LE (2006) Intermittency and the exchange of scalars in the nocturnal surface layer. *Boundary-Layer Meteorol* 119:41–55
- Acevedo OC, Moraes OLL, Fitzjarrald DR, Sakai RK, Mahrt L (2007) Turbulent carbon exchange in very stable conditions. *Boundary-Layer Meteorol* 125:49–61
- Anfossi D, Oettl D, Degrazia G, Goulart A (2005) An analysis of sonic anemometer observations in low wind speed conditions. *Boundary-Layer Meteorol* 114:179–203
- Banta RM, Pichugina YL, Brewer WA (2006) Turbulent velocity-variance profiles in the stable boundary layer generated by a nocturnal low-level jet. *J Atmos Sci* 63:2700–2719
- Businger JA (1973) Turbulent transfer in the atmospheric surface layer. In workshop on micrometeorology. *Am Met Soc* 84–87
- Chen J, Zhao CS, Ma N, Liu PF, Gobel T, Hallbauer E, Deng ZZ, Ran L, Xu WY, Liang Z, Liu HJ, Yan P, Zhou XJ, Wiedensohler A (2012) A parameterization of low visibilities for hazy days in the North China Plain. *Atmos Chem Phys* 12(11):4935–4950
- Chen R, Peng RD, Meng X, Zhou Z, Chen B, Kan H (2013) Seasonal variation in the acute effect of particulate air pollution on mortality in the China Air Pollution and Health Effects Study (CAPES). *Sci Total Environ* 450–451:259–265
- Coulter RL, Doran JC (2002) Spatial and temporal occurrences of intermittent turbulence during CASES-99. *Boundary-Layer Meteorol* 105(2):329–349
- Deng JJ, Wang TJ, Jiang ZQ, Xie M, Zhang RJ, Huang XX, Zhu JL (2011) Characterization of visibility and its affecting factors over Nanjing. *China Atmos Res* 101(3):681–691

- Ding YH, Liu YJ (2014) Analysis of long-term variations of fog and haze in China in recent 50 years and their relations with atmospheric humidity. *Sci China Earth Sci* 57:36–46
- Duntley SQ (1948) The reduction of apparent contrast by the atmosphere. *J Opt Soc Am* 38:179
- Elias T, Haefelin M, Drobinski P, Gomes L, Rangognio J, Bergot T, Chazette P, Raut JC, Colomb M (2009) Particulate contribution to extinction of visible radiation: pollution, haze, and fog. *Atmos Res* 92(4):443–454
- Fabbian D, de Dear R, Lelleyett S (2007) Application of artificial neural network forecasts to predict fog at Canberra International Airport. *Weather Forecast* 22(2):372–381
- Fu GQ, Xu WY, Yang RF, Li JB, Zhao CS (2014) The distribution and trends of fog and haze in the North China Plain over the past 30 years. *Atmos Chem Phys* 14:11949–11958
- Gao Y, Zhang M, Liu Z, Wang L, Wang P, Xia X, Tao M, Zhu L (2015) Modeling the feedback between aerosol and meteorological variables in the atmospheric boundary layer during a severe fog-haze event over the North China Plain. *Atmos Chem Phys* 15:4279–4295
- Gultepe I, Tardif R, Michaelides SC, Cermak J, Bott A, Bendix J, Muller MD, Pagowski M, Hansen B, Ellrod G, Jacobs W, Toth G, Cober SG (2007) Fog research: a review of past achievements and future perspectives. *Pure Appl Geophys* 164(6–7):1121–1159
- Han SQ, Liu JL, Hao TY, Zhang YF, Li PY, Yang JB, Wang QL, Cai ZY, Yao Q, Zhang M, Wang XJ (2018) Boundary layer structure and scavenging effect during a typical winter haze-fog episode in a core city of BTH region, China. *Atmos Environ* 179:187–200
- Helgason W, Pomeroy JW (2012) Characteristics of the near-surface boundary layer within a mountain valley during winter. *J Appl Meteorol Climatol* 51:583–597
- Hu XM, Ma Z, Lin W, Zhang H, Hu J, Wang Y, Xu X, Fuentes JD, Xue M (2014) Impact of the Loess Plateau on the atmospheric boundary layer structure and air quality in the North China Plain: a case study. *Sci Tot Environ* 499:228–237
- Huang N, Shen Z, Long S, Wu M, Shi H, Zheng Q, Yen N, Tung C, Liu H (1998) The empirical mode decomposition and the Hilbert spectrum for nonlinear and nonstationary time series analysis. *P R Soc A* 454:903–995
- Huang YX, Schmitt FG, Lu ZM, Liu YL (2008) An amplitude-frequency study of turbulent scaling intermittency using Empirical Mode Decomposition and Hilbert Spectral Analysis. *Europhys Lett* 84:40010
- Ji D, Wang Y, Wang L, Chen L, Hu B, Tang G, Xin J, Song T, Wen T, Sun Y, Pan Y, Liu Z (2012) Analysis of heavy pollution episodes in selected cities of northern China. *Atmos Environ* 50:338–348
- Ju TT, Wu BG, Wang ZY, Liu JL, Chen DH, Zhang HS (2020a) Relationships between low-level jet and low visibility associated with precipitation, air pollution, and fog in Tianjin. *Atmosphere* 11(11):1197
- Ju TT, Wu BG, Zhang HS, Liu JL (2020b) Characteristics of turbulence and dissipation mechanism in a polluted radiation-advection fog life cycle in Tianjin. *Meteorol Atmos Phys* 1–17
- Kim HJ, Collier S, Ge XL, Xu JZ, Sun YL, Jiang WQ, Wang YL, Herckes P, Zhang Q (2019) Chemical processing of water-soluble species and formation of secondary organic aerosol in fogs. *Atmos Environ* 200:158–166
- Li ZH, Liu D, Yang J, Pu MJ (2011) Physical and chemical characteristics of winter fogs in Nanjing. *Acta Meteorol Sin* 69:706–718
- Li XL, Hu XM, Ma YJ, Wang YF, Li LG, Zhao ZQ (2019) Impact of planetary boundary layer structure on the formation and evolution of air pollution episodes in Shenyang, Northeast China. *Atmos Environ* 214:116850
- Liu Z, Hu B, Wang L, Wu F, Gao W, Wang Y (2014) Seasonal and diurnal variation in particulate matter (PM₁₀ and PM_{2.5}) at an urban site of Beijing: analyses from a 9-year study. *Environ Sci Pollut Res* 22:627–642
- Liu L, Zhang X, Zhong J, Wang J, Yang Y (2019) The ‘two-way feedback mechanism’ between unfavorable meteorological conditions and cumulative PM_{2.5} mass existing in polluted areas south of Beijing. *Atmos Environ* 208:1–9
- Mahrt L (1989) Intermittency of atmospheric turbulence. *J Atmos Sci* 46:79–95
- Mahrt L (1998) Nocturnal boundary-layer regimes. *Boundary-Layer Meteorol* 88:255–278
- Mahrt L (1999) Stratified atmospheric boundary layers. *Boundary-Layer Meteorol* 90(3):375–396
- Mahrt L (2007) The influence of nonstationarity on the turbulent flux-gradient relationship for stable stratification. *Boundary-Layer Meteorol* 125(2):245–264
- Mahrt L (2010) Variability and maintenance of turbulence in the very stable boundary layer. *Boundary-Layer Meteorol* 135(1):1–18
- Mahrt L (2014) Stably stratified atmospheric boundary layers. *Annu Rev Fluid Mech* 46:23–45
- Miao YC, Guo JP, Liu S, Zhao C, Li X, Zhang G, Wei W, Ma Y (2018) Impacts of synoptic condition and planetary boundary layer structure on the trans-boundary aerosol transport from Beijing–Tianjin–Hebei region to Northeast China. *Atmos Environ* 181:1–11

- Petäjä T, Järvi L, Kerminen VM, Ding AJ, Sun JN, Nie W, Kujansuu J, Virkkula A, Yang X, Fu CB, Zilitinkevich S, Kulmala M (2016) Enhanced air pollution via aerosol-boundary layer feedback in China. *Sci Rep* 6:18998
- Quan J, Zhang Q, He H, Liu J, Huang M, Jin H (2011) Analysis of the formation of fog and haze in North China Plain (NCP). *Atmos Chem Phys* 11(15):8205–8214
- Ren Y, Zhang HS, Wei W, Wu BG, Cai XH, Song Y (2019a) Effects of turbulence structure and urbanization on the heavy haze pollution process. *Atmos Chem Phys* 19:1041–1057
- Ren Y, Zhang HS, Wei W, Wu BG, Liu JL, Cai XH, Song Y (2019b) Comparison of the turbulence structure during light and heavy haze pollution episodes. *Atmos Res* 230:104645
- Ren Y, Zhang HS, Zhang XY, Wei W, Li QH, Wu BG, Cai XH, Song Y, Kang L, Zhu T (2021) Turbulence barrier effect during heavy haze pollution events. *Sci Tot Environ* 753:142286
- Salmond JA (2005) Wavelet analysis of intermittent turbulence in a very stable nocturnal boundary layer: implications for the vertical mixing of ozone. *Boundary-Layer Meteorol* 114:463–488
- Sorbjan Z, Czerwinska A (2013) Statistics of turbulence in the stable boundary layer affected by gravity waves. *Boundary-Layer Meteorol* 148:73–91
- Sun J, Lenschow DH, Burns SP, Banta RM, Newsom RK, Coulter R, Frasier S, Ince T, Nappo C, Balsley BB, Jensen M, Mahrt L, Miller D, Skelly B (2004) Atmospheric disturbances that generate intermittent turbulence in nocturnal boundary layers. *Boundary-Layer Meteorol* 110:255–279
- Sun Y, Jiang Q, Wang Z, Fu P, Li J, Yang T, Yin Y (2014) Investigation of the sources and evolution episodes of severe haze pollution in Beijing in January 2013. *J Geophys Res Atmos* 119:4380–4398
- Tang G, Zhang J, Zhu X, Song T, Munkel C, Hu B, Schäfer K, Liu Z, Zhang J, Wang L, Xin J, Suppan P, Wang Y (2016) Mixing layer height and its implications for air pollution over Beijing, China. *Atmos Chem Phys* 16:2459–2475
- Tao M, Chen L, Xiong X, Zhang M, Ma P, Tao J, Wang Z (2014) Formation process of the widespread extreme haze pollution over northern China in January 2013: implications for regional air quality and climate. *Atmos Environ* 98:417–425
- Terradellas E, Soler MR, Ferreres E, Bravo M (2005) Analysis of oscillations in the stable atmospheric boundary layer using wavelet methods. *Boundary-Layer Meteorol* 114:489–518
- Tian M, Wu BG, Huang H, Zhang HS, Zhang WY, Wang ZY (2019) Impact of water vapor transfer on a Circum-Bohai-Sea heavy fog: Observation and numerical simulation. *Atmos Res* 229:1–22
- Van de Wiel BJH, Moene AF, Hartogensis OK, De Bruin HAR, Holtslag AAM (2003) Intermittent turbulence in the stable boundary layer over land. Part III: A classification for observations during CASES-99. *J Atmos Sci* 60:2509–2522
- Vickers D, Mahrt L (2006) A solution for flux contamination by mesoscale motions with very weak turbulence. *Boundary-Layer Meteorol* 118:431–447
- Vindel JM, Yagüe C (2011) Intermittency of turbulence in the atmospheric boundary layer: Scaling exponents and stratification influence. *Boundary-Layer Meteorol* 140:73–85
- Wang ZB, Hu M, Wu ZJ, Yue DL, He LY, Huang XF, Liu XG, Wiedensohler A (2013) Long-term measurements of particle number size distributions and the relationships with air mass history and source apportionment in the summer of Beijing. *Atmos Chem Phys* 13:10159–10170
- Wang J, Wang S, Jiang J, Ding A, Zheng M, Zhao B, Wong DC, Zhou W, Zheng G, Wang L, Pleim JE, Hao J (2014) Impact of aerosol–meteorology interactions on fine particle pollution during China’s severe haze episode in January 2013. *Environ Res Lett* 9:094002
- Wang H, Peng Y, Zhang XY, Liu HL, Zhang M, Che HZ, Cheng YL, Zheng Yu (2018) The contributions to the explosive growth of PM_{2.5} mass due to aerosols-radiation feedback and further decrease in turbulent diffusion during a red-alert heavy haze in JING-JIN-JI in China. *Atmos Chem Phys* 18:17717–17733
- Wei W, Zhang HS, Ye XX (2014) Comparison of low-level jets along the north coast of China in summer. *J Geophys Res Atmos* 119(16):9692–9706
- Wei W, Schmitt FG, Huang YX, Zhang HS (2016) The analyses of turbulence characteristics in the atmospheric surface layer using arbitrary-order Hilbert spectra. *Boundary-Layer Meteorol* 159:391–406
- Wei W, Wang M, Zhang HS, He Q, Ali M, Wang Y (2017) Diurnal characteristics of turbulent intermittency in the Taklimakan Desert. *Meteorol Atmos Phys* 131:287–297
- Wei W, Zhang HS, Wu BG, Huang YX, Cai XH, Song Y, Liu JL (2018) Intermittent turbulence contributes to vertical diffusion of PM_{2.5} in the North China Plain: cases from Tianjin. *Atmos Chem Phys* 18:12953–12967
- WMO (1992) International meteorological vocabulary. Geneva WMO, pp 1–276.
- Wu BG, Li ZF, Ju TT, Zhang HS (2020) Characteristics of low-level jets during 2015–2016 and the effect on fog in Tianjin. *Atmos Res* 105102
- Ye XX, Wu BG, Zhang HS (2015a) The turbulent structure and transport in fog layers observed over the Tianjin area. *Atmos Res* 153:217–234

- Ye XX, Song Y, Cai XH, Zhang HS (2015b) Study on the synoptic flow patterns and boundary layer process of the severe haze events over the North China Plain in January 2013. *Atmos Environ* 124:129–145
- Zhang XY, Wang YQ, Niu T, Zhang XC, Gong SL, Zhang YM, Sun JY (2012) Atmospheric aerosol compositions in China: spatial/temporal variability, chemical signature, regional haze distribution and comparisons with global aerosols. *Atmos Chem Phys* 12:779–799
- Zhang L, Sun JY, Shen XJ, Zhang YM, Che H, Ma QL, Zhang YW, Zhang XY, Ogren JA (2015) Observations of relative humidity effects on aerosol light scattering in the Yangtze River Delta of China. *Atmos Chem Phys* 15:8439–8454
- Zhao XJ, Zhao PS, Xu J, Meng W, Pu WW, Dong F, He D, Shi QF (2013) Analysis of a winter regional haze event and its formation mechanism in the North China Plain. *Atmos Chem Phys* 13(11):5685–5696
- Zhong JT, Zhang XY, Dong YS, Wang YQ, Liu C, Wang JZ, Zhang YM, Che HC (2018) Feedback effects of boundary-layer meteorological factors on cumulative explosive growth of PM_{2.5} during winter heavy pollution episodes in Beijing from 2013 to 2016. *Atmos Chem Phys* 18(1):247–258

Publisher's Note Springer Nature remains neutral with regard to jurisdictional claims in published maps and institutional affiliations.